Support information

Theoretical insight into the opposite redox activity of iron complexes toward the ring opening polymerization of lactide and epoxide

Xiaowei Xu,[a] Han Lu,[a] Gen Luo,[b] Xiaohui Kang,[c] Yi Luo*[a]

[a]*State Key Laboratory of Fine Chemicals, School of Chemical Engineering, Dalian University of Technology, Dalian 116024, China*

[b]*Institutes of Physical Science and Information Technology, Anhui University, Hefei 230601, China*

[c]*College of Pharmacy, Dalian Medical University, Dalian, Liaoning 116044, China*

Contents

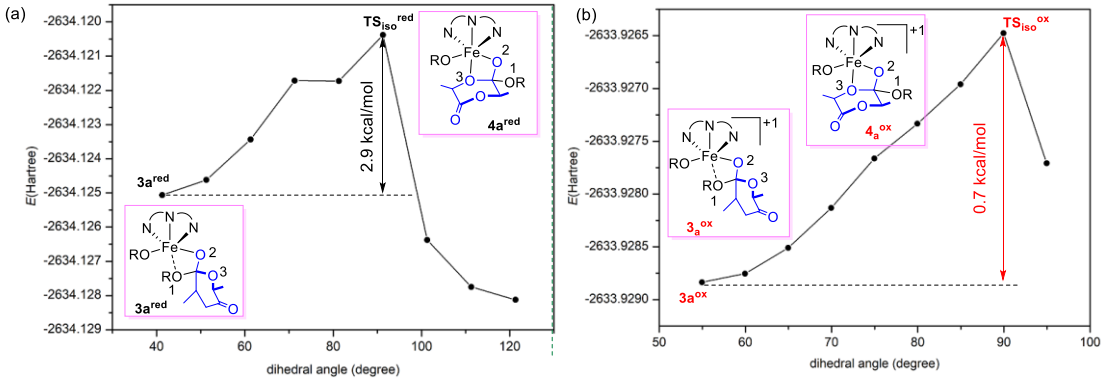

Fig. S1 Relaxed scan of potential energy surfaces (PES) for the dihedral angle of Fe-O2-C-O1 in $\mathbf{3a^{red}}$ / $\mathbf{3a^{ox}}$ at the DFT/BSI level.

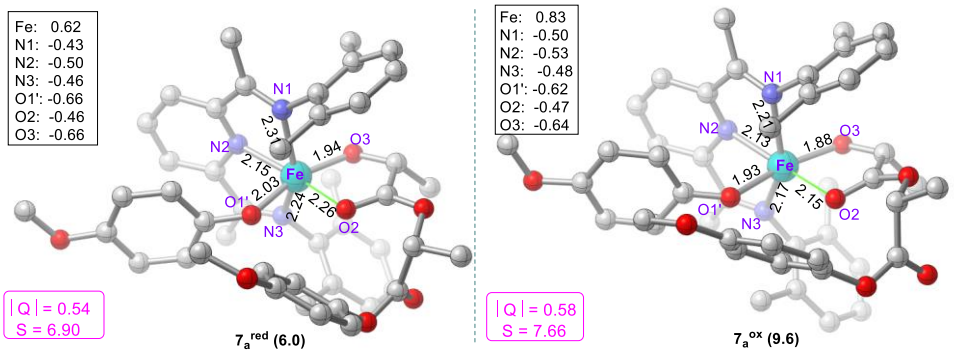

Fig. S2 Optimized structures (distances in Å) of the insertion and ring-opening products ($\mathbf{7a^{red}}$ and $\mathbf{7a^{ox}}$) of the first monomer. Values in parentheses are the Gibbs free energies (kcal mol^{-1}) in solution relative to isolated reactants. Mulliken atomic charges are given for important atoms, viz., Fe, N1, N2, N3, O1′, O2, and O3 atoms. |Q| and S denote the unsigned average value and square error of the charge ($S = \Sigma(|Q_x| - |Q|)^2$), respectively. Q*x* denotes the charge on the individual atoms.

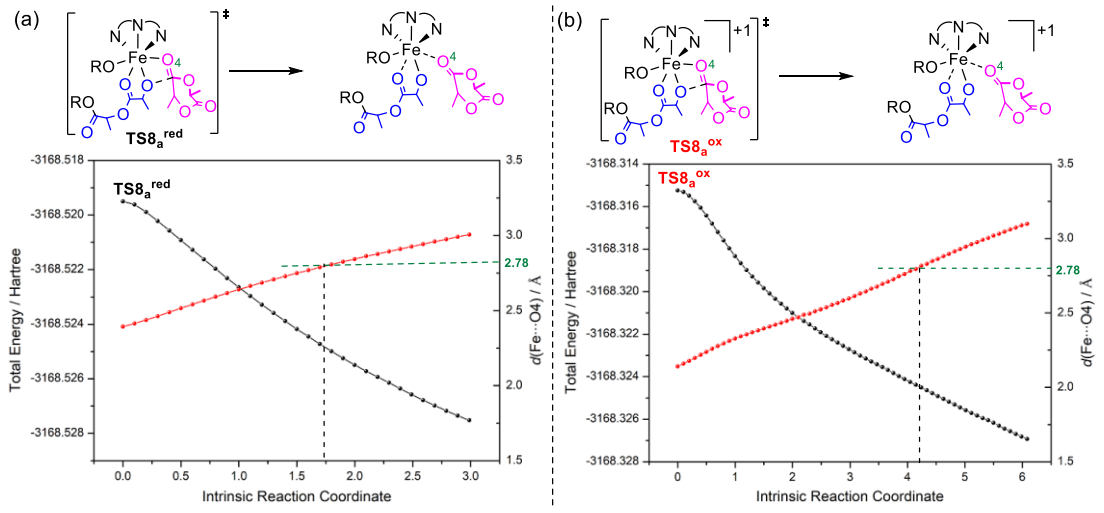

Fig. S3 IRC following (black line) of $\mathbf{TS8a^{red}}$ (a) and $\mathbf{TS8a^{ox}}$ (b) and the energy change

with the elongation of Fe···O4 distance (red line). The area of coordination complex was not found until the distance of Fe···O4 reaches the sum of van der Waals radii of Fe and O atoms (2.78 Å).

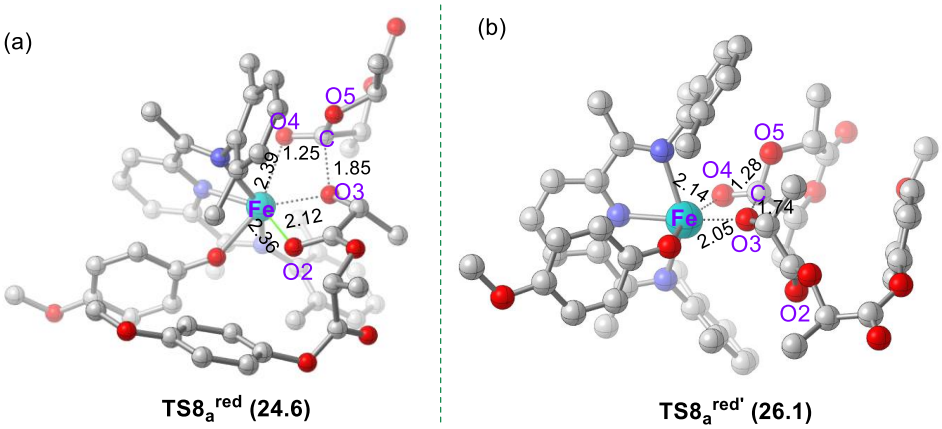

Fig. S4 Migration insertion transition states for the second LA insertion. (a), **TS8a^{red}** with a chelating interaction with the carbonyl of the last inserted lactic acid unit. (b), **TS8a$^{red'}$** with dissociation of the carbonyl prior to insertion of an incoming monomer. Values in parentheses are the relative Gibbs free energy barriers. Energies are given in kcal mol^{-1}.

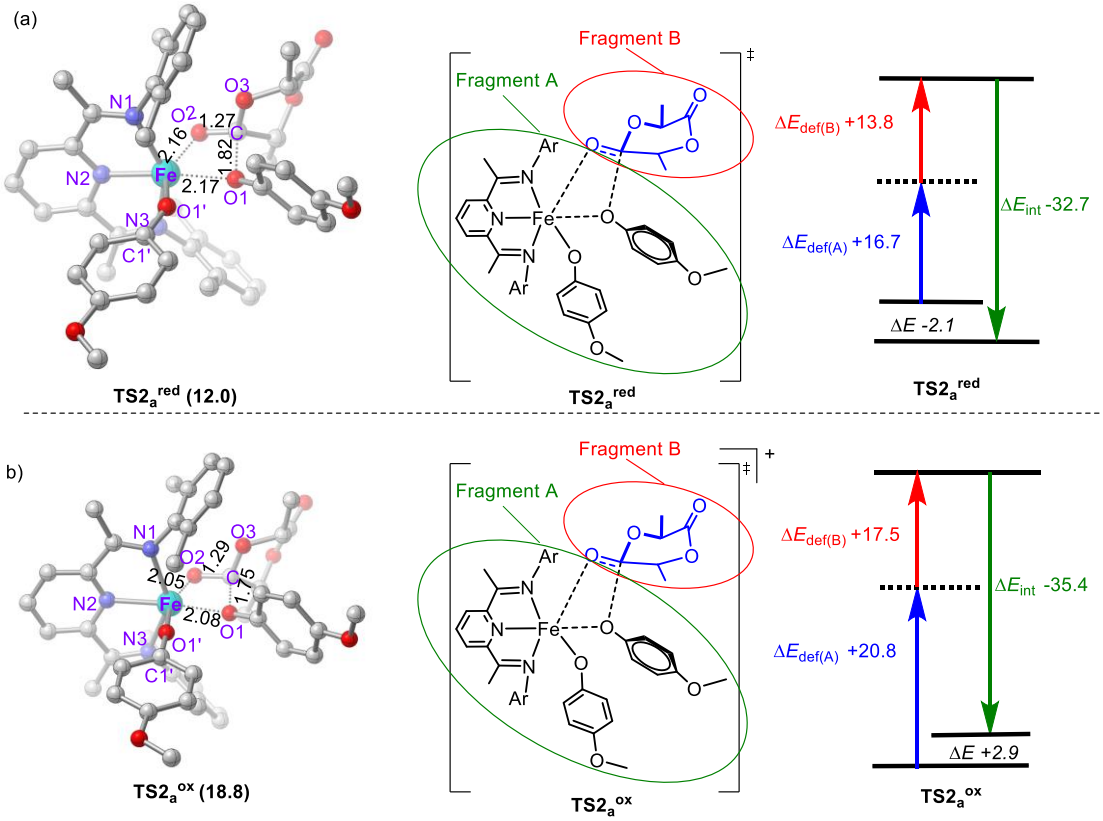

Fig. S5 Optimized geometries (distances in Å) and distortion/interaction analysis (kcal mol^{-1}) of **TS2a^{red}** and **TS2a^{ox}**. Values in parentheses are the relative Gibbs free energy barriers.

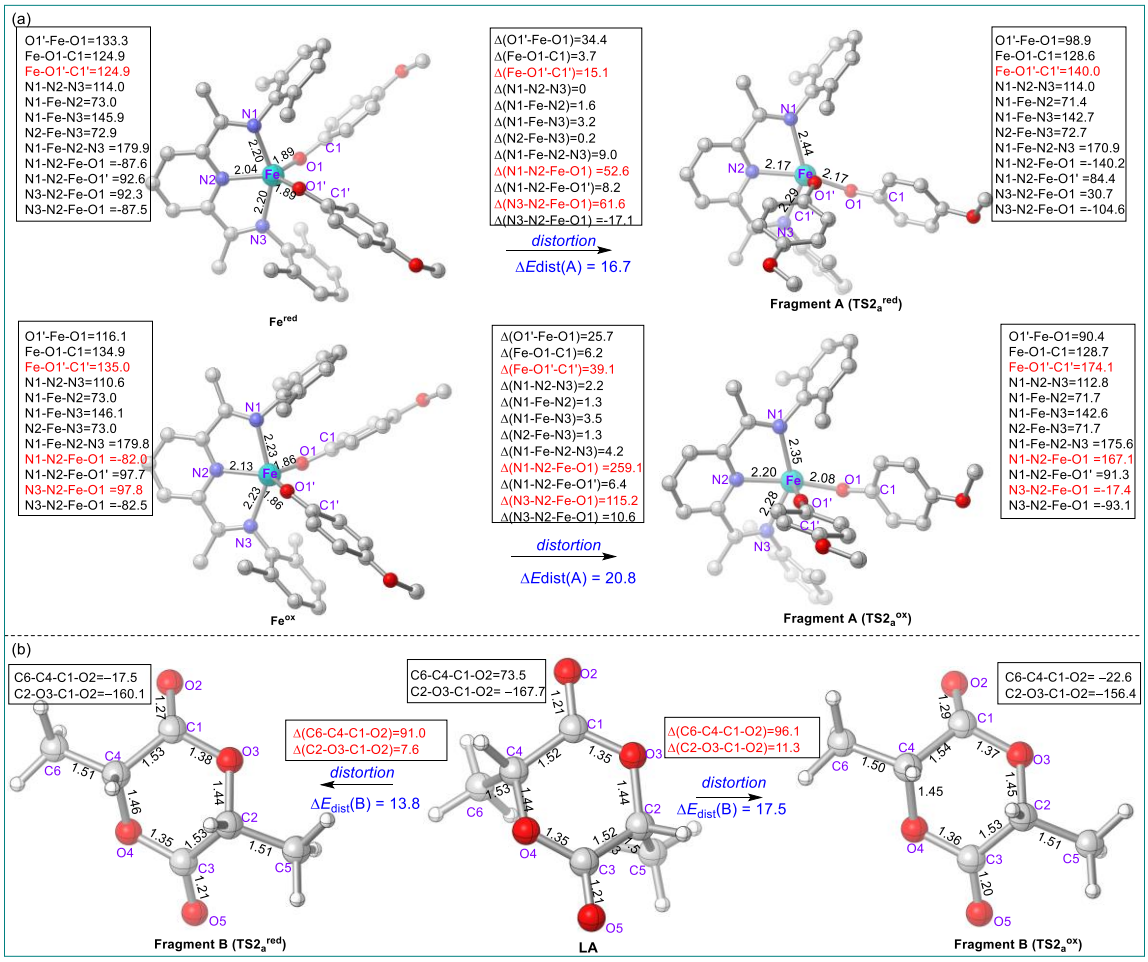

Fig. S6 Geometrical comparison of the two fragments in distortion/interaction analysis. (a) Fragment A in **TS2a^{red}** relative to **Fe^{red}** and fragment A in **TS2a^{ox}** relative to **Fe^{ox}**. (b) Fragment B in **TS2a^{red}** and fragment B in **TS2a^{ox})** relative to monomer LA. The distances are in angstroms and angles are in degree. Energies are given in kcal mol^{-1}.

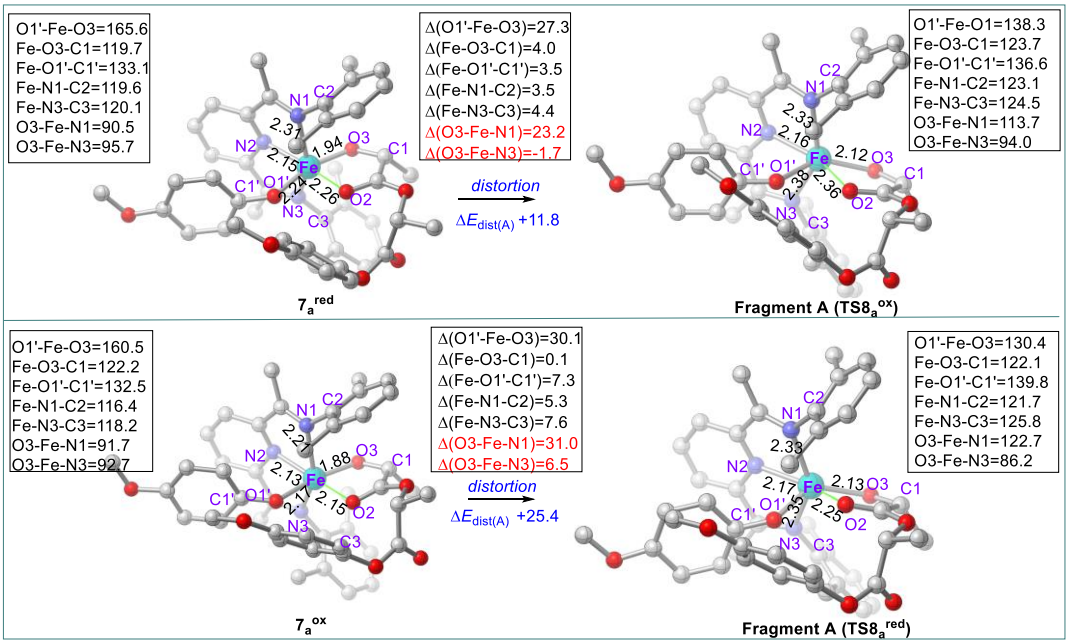

Fig. S7 Geometrical comparison of the fragment A in **TS8a^{red}** relative to **7a^{red}** and the fragment A in **TS8a^{ox}** relative to **7a^{ox}**. The distances are in angstroms and angles are in degree. Energies are given in kcal mol^{-1}.

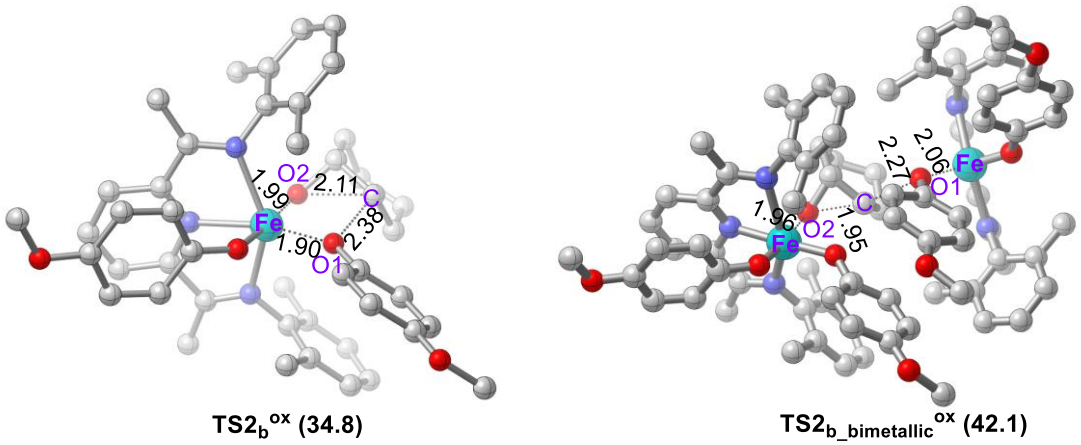

Fig. S8 Transition states for the CHO insertion in the mono-metallic (a) and bimetallic system (b) at the level of (PCM, solvent=chlorobenzene) B3LYP-D3BJ/Lanl2dz(Fe)/6-311+G**(other atoms)//B3LYP-D3BJ/Lanl2dz(Fe)/3-21G*(other atoms). The free energy barrier (kcal mol^{-1}) are given in parentheses.

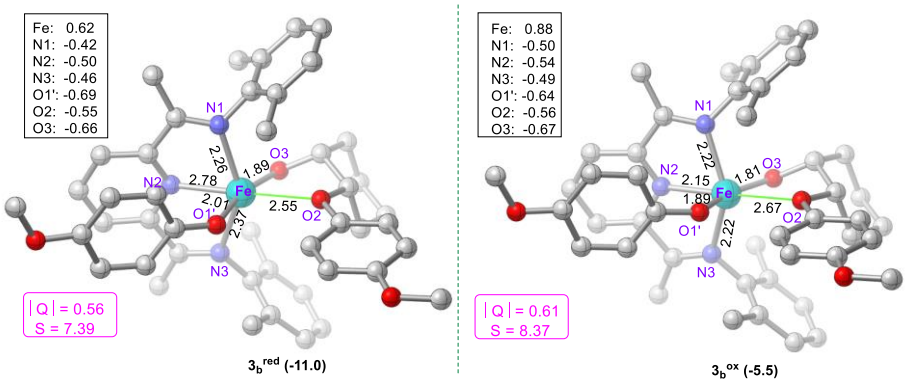

Fig. S9 Optimized structures (distances in Å) of the insertion and ring-opening products ($\mathbf{3_b^{red}}$ and $\mathbf{3_b^{ox}}$) of the first monomer. Values in parentheses are the Gibbs free energies (kcal mol^{-1}) in solution relative to isolated reactants. Mulliken atomic charges are given for important atoms, viz., Fe, N1, N2, N3, O1′, O2, and O3. |Q| and S denote the unsigned average value and square error ($S = \Sigma(|Q_x| - |Q|)^2$) of the charges, respectively. Q*x* denotes the charge on individual atoms.

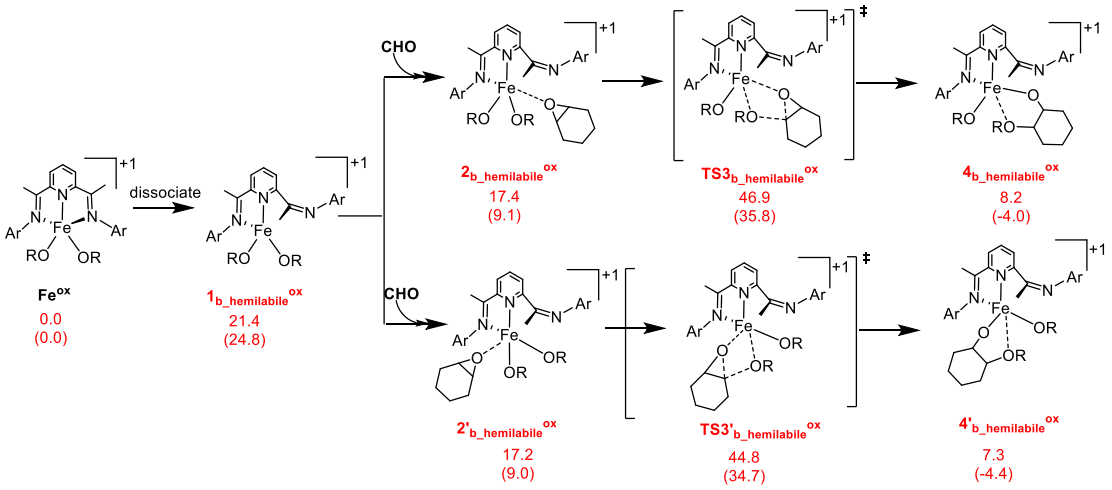

Fig. S10 Computed energy profiles for CHO polymerization involving hemilabile bis(imino)pyridine ligands. The enthalpy values are given in parentheses. Free energies (kcal mol^{-1}) are relative to the energy sum of isolated reactants.

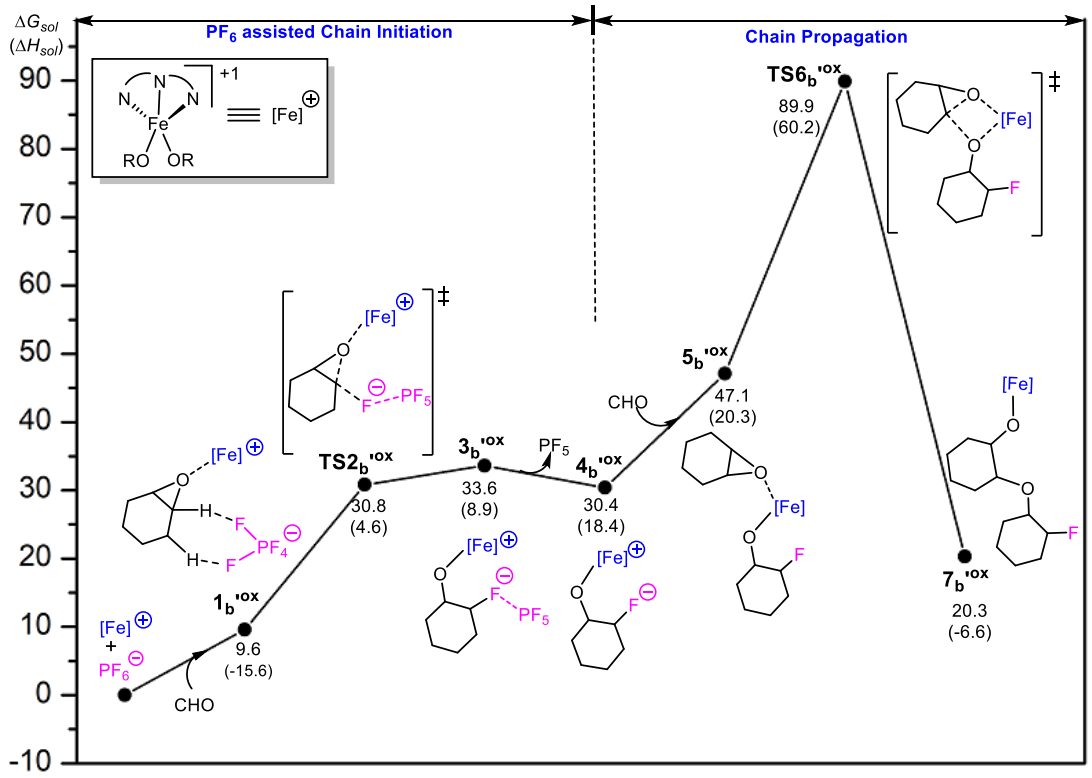

Fig. S11 Computed energy profiles for CHO polymerization with $PF6^-$ assistance. The enthalpy values are given in parentheses. Free energies (kcal mol^{-1}) are relative to the energy sum of isolated reactants.

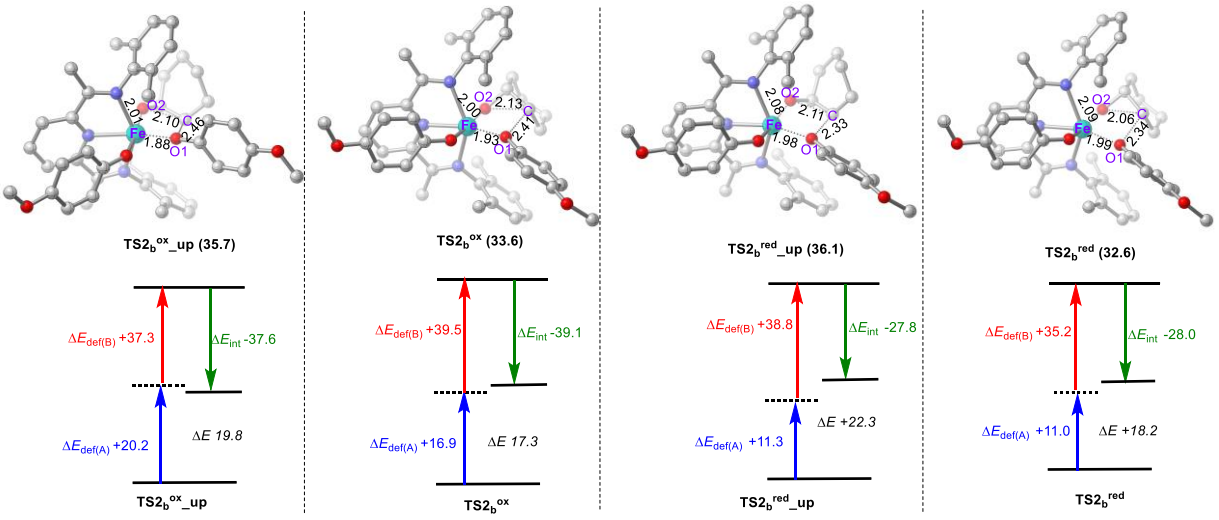

Fig. S12 Optimized geometries (distances in Å) and distortion/interaction analyses (kcal mol^{-1}) for the CHO ring-opening transition states with different insertion fashion. The values of free energy barrier are given in parentheses.

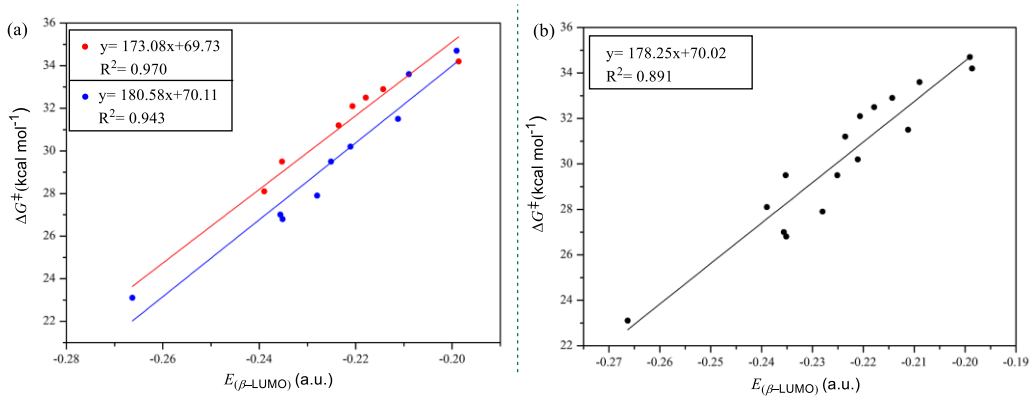

Fig. S13 Relationship between the free energy barrier ($\Delta G^{\ddagger}$, in kcal mol^{-1}) of rate-determination step for CHO enchainment *versus* LUMO energy ($E_{(\beta\text{-LUMO})}$) of corresponding complexes. (a) Red dots stand for the iron analogues (**Fe^{ox}**, **O^{ox}**, and **A^{ox}**→**G^{ox}**) with various *para*-substituent on phenoxyl and blue dots represent the iron complexes (**Fe^{ox}**, and **H^{ox}**→**O^{ox}**) with different substituents on the backbone of bis(imino)pyridine ligand. (b) Black dots stand for the all proposed iron complexes (**A^{ox}**→**O^{ox}**) and **Fe^{ox}**.

Table S1 Relative electronic energies (ΔE, kcal/mol) of various spin states of active species.

catalyst	spin states	ΔE	catalyst	spin states	ΔE
Fe^{red}	singlet (closed-shell)	0.0	**Fe^{ox}**	doublet	0.0
	singlet (open-shell)	0.0		quartet	-32.0
	triplet	-6.7		sextet	-41.5
	quintet	-33.9		Octet	-4.4
	septet	-12.3			

Table S2 Free energies (kcal mol^{-1}) for coordination complexes (**1b$_{ox}$**) and ring-opening TSs (**TS2b$_{ox}$**) for modelled iron complexes analogous. Free energy barriers ($\Delta G^{‡}$,kcal mol^{-1}) are relative to the energy sum of isolated reactants.

System	**1b$_{ox}$**	**TS2b$_{ox}$**	$\Delta G^{‡}$
A^{ox}+CHO	6.1	34.2	34.2
B^{ox}+CHO	8.3	32.9	32.9
C^{ox}+CHO	8.5	32.5	32.5
D^{ox}+CHO	8.3	32.1	32.1
E^{ox}+CHO	8.2	31.2	31.2
F^{ox}+CHO	7.3	29.5	29.5
G^{ox}+CHO	6.4	28.1	28.1
H^{ox}+CHO	11.3	34.7	34.7
I^{ox}+CHO	6.5	31.5	31.5
J^{ox}+CHO	3.3	30.2	30.2
K^{ox}+CHO	3.4	29.5	29.5
L^{ox}+CHO	1.7	27.9	27.9
M^{ox}+CHO	1.2	27.0	27.0
N^{ox}+CHO	0.3	26.8	26.8
O^{ox}+CHO	0.8	23.1	23.1